# High Carrier Mobility and Pronounced Light Absorption in Methyl-Terminated Germanene: Insights from First-Principles Computations

**ARTICLE** *in* JOURNAL OF PHYSICAL CHEMISTRY LETTERS · OCTOBER 2015

Impact Factor: 7.46 · DOI: 10.1021/acs.jpclett.5b01848



**5 AUTHORS**, INCLUDING:

Yu Jing

Nankai University

**14** PUBLICATIONS **313** CITATIONS

SEE PROFILE

Xu Zhang

Nankai University

**7** PUBLICATIONS **9** CITATIONS

SEE PROFILE

Zhen Zhou

Nankai University

**213** PUBLICATIONS **6,983** CITATIONS

SEE PROFILE

THE JOURNAL OF PHYSICAL CHEMISTRY Letters

Letter

pubs.acs.org/JPCL

# High Carrier Mobility and Pronounced Light Absorption in Methyl-Terminated Germanene: Insights from First-Principles Computations

Yu Jing, Xu Zhang, Dihua Wu, Xudong Zhao, and Zhen Zhou*

Tianjin Key Laboratory of Metal and Molecule Based Material Chemistry, Key Laboratory of Advanced Energy Materials Chemistry (Ministry of Education), Computational Centre for Molecular Science, Institute of New Energy Material Chemistry, Collaborative Innovation Center of Chemical Science and Engineering (Tianjin), School of Materials Science and Engineering, National Institute for Advanced Materials, Nankai University, Tianjin 300353, P. R. China

Supporting Information

**ABSTRACT:** On the basis of Herd–Scuseria–Emzerhof hybrid functional (HSE06) within the framework of density functional theory (DFT), we have computationally explored the intrinsic electronic and optical properties of 2D methyl-terminated germanene ($GeCH_3$). $GeCH_3$ monolayer possesses an opportune direct band gap of 1.76 eV, which can be effectively tuned by applying elastic strain and decreases with increasing the tensile strain, while it increases with small compressive strain. Also, anisotropic carrier mobility was disclosed in the armchair ($x$) and zigzag ($y$) directions of $GeCH_3$ monolayer. Moreover, $GeCH_3$ monolayer shows significant light absorption in the visible and ultraviolet range of solar spectrum and is attractive for light harvesting. The results can help us better understand the intrinsic properties of $GeCH_3$ and provide reliable guidance for its experimental applications to electronics and optoelectronics.

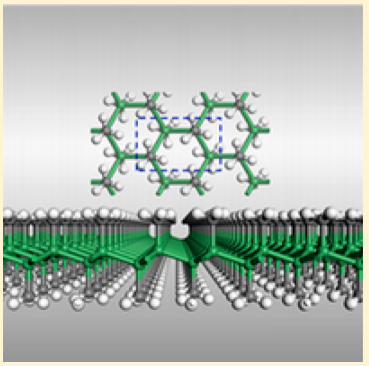

In the past decade, graphene has won enormous research enthusiasm and boomed the development of 2D materials for electronics and energy storage.[1−6] One of the most fascinating properties of graphene is its extremely high carrier mobility (200 000 $cm^2/(V\ s)$),[7,8] which can endow electronic devices with high drive current and low intrinsic delay; however, the character of zero band gap in graphene has severely limited its applications in microelectronic devices. Hence, great efforts have been devoted to either opening an appropriate band gap in graphene or searching for other 2D materials with favorable carrier mobility and opportune band gap.

Surface functionalization is an effective approach to tune the band structure of graphene.[9] The band gap of graphene can be enlarged by saturation with different surface terminations. Fully H- and F-terminated graphene, termed as graphane and fluoride graphane, respectively, can maintain the flatness and strength of graphene;[10] however, both turn out to be insulators with large band gaps, and the great electron mobility of graphene is missing in graphane and fluoride graphane.[11] Although theoretical investigations predicted that the electronic properties of graphane and fluoride graphane can be appropriately modified via interlayer hydrogen or halogen bonding,[12] the fabrication process is difficult to be performed in the laboratory.

Other 2D materials, including but not limited to single-layered transition-metal chalcogenides (such as $MoS_2$ and $WS_2$), $h$-BN, silicene, germanene, MXene, and phosphorene, have also been extensively explored.[13−17] Among those graphene analogs, $MoS_2$ shows appropriate band gap but low carrier mobility,[18] while phosphorene shows applicable band gap and high carrier mobility but poor stability.[19] Silicene and germanene have also attracted much research enthusiasm because they are structure analogs and isoelectronic species of graphene. As expected, silicene and germanene exhibit extremely similar electronic properties to graphene, including quantum spin Hall effect, low effective masses, and high carrier mobility;[20−24] however, the negligible band gap of silicene and germanene has also restricted their applications to electronics.[25,26]

Recently, Bianco et al. have experimentally obtained single- and few-layer hydrogen terminated germanene, namely germanane (GeH) on $SiO_2$/Si surfaces, via a mechanical exfoliation method.[27,28] As demonstrated by both theoretical and experimental investigations, GeH is an attractive semiconductor with a direct band gap of ∼1.59 eV and shows low effective mass.[29] Therefore, surface termination with hydrogen turns out to be an effective method in opening a beneficial band gap for germanene without conceding its low effective mass. The opportune band gap and low effective mass make GeH rather attractive for electronics and optoelectronics;[30] however, GeH shows low thermal stability that is not favorable for electronics, and thus other possible surface terminations for germanene come to researchers' attention.

Very recently, Jiang et al. have converted $CaGe_2$ crystals into millimeter-sized $GeCH_3$ through a facile, one-step metathesis

**Received:** August 24, 2015
**Accepted:** October 11, 2015

  

DOI: 10.1021/acs.jpclett.5b01848
J. Phys. Chem. Lett. 2015, 6, 4252−4258

approach.[31] By replacing H-termination with $CH_3-$ in GeH, one can prepare $GeCH_3$ favorably. Possessing good resistance to oxidation akin to GeH, $GeCH_3$ exhibits strong photoluminescence effects and thickness-independent band-edge fluorescence. Meanwhile $GeCH_3$ shows enhanced thermal stability compared with GeH and can be stable up to 250 °C. These fantastic properties make $GeCH_3$ more attractive for electric and optical applications; however, the specific electronic properties (especially the carrier mobility) and optical properties of $GeCH_3$ are still vague.

Driven by the above questions, we performed first-principles computations to investigate the intrinsic electronic and optical properties of 2D $GeCH_3$ on the basis of density functional theory (DFT). We found that $GeCH_3$ monolayer is semiconducting with a direct band gap, which can be effectively tuned by applying tensile and compressive strain from the uniaxial and biaxial directions. Spin−orbit coupling (SOC) effect was found feebly to change the band gap of $GeCH_3$ but can alter the effective hole masses along the armchair and zigzag directions. Involving SOC effect, our DFT computations demonstrate that $GeCH_3$ possesses anisotropic effective masses along the armchair and zigzag directions and exhibits high carrier mobility along the armchair direction. Meanwhile, we also explored the optical properties of $GeCH_3$ and found that $GeCH_3$ shows strong absorption in the visible and ultraviolet range of solar spectrum and thus is promising for light harvesting. These fantastic electronic and optical properties endow $GeCH_3$ with great potentials for electronic and optoelectronic devices.

In this work, first-principles computations on the basis of DFT were performed on 2D $GeCH_3$ hexagonal/orthogonal lattice by using Vienna ab initio simulation package (VASP).[32] Projector-augmented plane wave (PAW) approach was applied to describe the ion−electron interactions.[33,34] We performed the generalized gradient approximation (GGA) involving PBE +D2 (PBE is the abbreviation of the functional of Perdew, Burke, and Ernzerhof, and D stands for dispersion) method and the Grimme vdW correction, which can accurately describe the weak interactions.[35,36] By using the conjugated gradient method, geometry optimizations were performed with a convergence threshold of $10^{-4}$ eV in energy and $10^{-2}$ eV/Å in force. The k-point mesh of the Brillouin zone was set to be 16 × 10 × 1 for geometry optimization. Electronic and optical properties were further calculated by the Herd−Scuseria−Emzerhof hybrid functional (HSE06).[37] A 500 eV cutoff energy for the plane-wave basis set was adopted in all computations. Phonon spectra were computed by means of linear response method as implemented in CASTEP code.[38]

For inorganic semiconductors, the electron coherence length is close to the acoustic phonon wavelength and is longer than the bonds. Thus, the phonon scattering dominates the intrinsic mobility and can be described by the deformation potential (DP) theory,[39] which is a simple approximation of the full Boltzmann transport equation and has proved effective in predicting the carrier mobility of 2D semiconductors like $MoS_2$, phosphorene, MXene, and so on.[18,19,40−42] Therefore, the carrier mobility ($\mu$) of 2D $GeCH_3$ is predicted through the phonon limited scattered mode and calculated on the basis of effective mass approximation by using the DP theory, according to eq 1

$$\mu = \frac{2e\hbar^3 C}{3k_B T|m^*|^2 E_1^{\,2}} \tag{1}$$

In this equation, $\hbar$ is reduced Planck constant, $k_B$ is Boltzmann constant, and $T$ is the temperature, while $m^*$, $E_1$, and $C$ are the effective mass, DP constant, and in-plane stiffness of the studied 2D material, respectively. $T$ is set to be 300 K, corresponding to room temperature. Parameters $m^*$, $E_1$, and $C$ for 2D $GeCH_3$ can be acquired by first-principles computations and will be discussed in detail. SOC effect was involved during the calculation of $m^*$ and $E_1$.

The imaginary part $\varepsilon_2(\omega)$ of dielectric function can be expressed by eq 2[43]

$$\varepsilon_{\alpha\beta}^2(\omega) = \frac{4\pi^2 e^2}{\Omega}\lim_{q\to 0}\frac{1}{q^2}\sum_{c,v,\vec{k}} 2w_{\vec{k}}\delta(\varepsilon_{c\vec{k}} - \varepsilon_{v\vec{k}} - \omega) \times \langle u_{c\vec{k}+e_\alpha\vec{q}}|u_{v\vec{k}}\rangle\langle u_{c\vec{k}+e_\beta\vec{q}}|u_{v\vec{k}}\rangle^* \tag{2}$$

in which $c$ and $v$ refer to the conduction and valence band states, respectively, both of which were determined by the HSE06 functional in this work, and $u_{c\vec{k}}$ is the cell periodic part of the orbitals at the k-point $\vec{k}$.

Elastic strain along $x$ and $y$ directions in the range of −2∼5% was simulated to tune the band gap of $GeCH_3$, corresponding to the compressive and tensile strain, respectively. The strain ($\varepsilon$) is defined as $\varepsilon = (a - a_0)/a_0$, while $a$ is the strained lattice parameter and $a_0$ is the equilibrium lattice constant (along $x$ or $y$ directions). As a comparison, biaxial strain along both $x$ and $y$ directions was also taken in to account for the modulation of the band structure.

*Intrinsic Structural and Electronic Properties of $GeCH_3$.* The structural properties of $GeCH_3$ monolayer were explored first. The supercell in the original hexagonal lattice is provided in Figure 1a. The optimized lattice constant $a$ is 4.00 Å for $GeCH_3$ in a hexagonal unit cell as enclosed in the red dashed lines in Figure 1a, in good accordance with the previous experimental report ($a$ = 3.97 Å).[31] The orthogonal lattice denoted in the blue dashed lines is applied in this study for the convenience of demonstrating the carrier mobility along the armchair ($x$) and

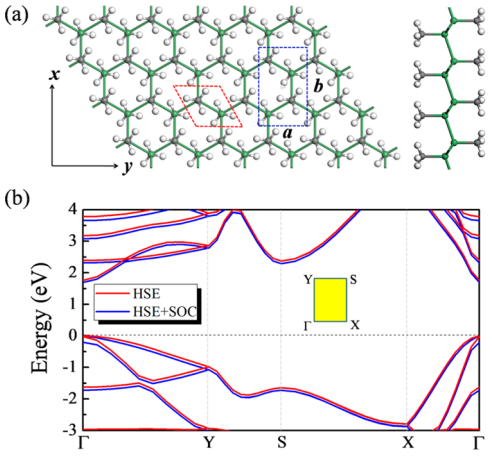


**Figure 1.** (a) Structure schematics of $GeCH_3$ monolayer in a 4 × 6 supercell from the top and side views, and the hexagonal primitive cell and the orthogonal supercell are enclosed in the red and blue dashed lines, respectively. (b) Band structure of $GeCH_3$ monolayer computed at the HSE06 level with and without SOC effect. The first Brillouin zone for an orthogonal lattice is plotted inside. The valence band maximum (VBM) is set to be the Fermi level, which is denoted with a dark dashed line.



DOI: 10.1021/acs.jpclett.5b01848
J. Phys. Chem. Lett. 2015, 6, 4252−4258

zigzag ($y$) directions. To avoid any interlayer interactions, the lattice in the $z$ direction of $GeCH_3$ is set to be 25 Å.

As shown in Figure 1a, the $CH_3-$ groups bonded to Ge atoms spread alternatively in the up and down sides of Ge bilayer, contributing to the full termination of Ge surface in $GeCH_3$. In the case of GeH, there are two possible planar configurations, the chair and boat morphologies.[29] As demonstrated by Ghosh et al., the chair configuration of GeH has both large band gap and low effective mass, which are attractive for switching device applications; however, for $GeCH_3$, due to the large steric hindrance of $CH_3-$, the boat configuration is excluded and the favorable chair configuration is illustrated in Figure 1a. The lengths of Ge−Ge and Ge−C bonds are 2.44 and 2.00 Å, respectively. The bond angle of H−C−H in the $CH_3-$ groups is ∼109°. To estimate the stability of $GeCH_3$, we performed phonon calculation. As shown in Figure S1a (Supporting Information), there are no imaginary phonon modes in the phonon spectrum of $GeCH_3$, indicating the good kinetic stability of $GeCH_3$.

With such fantastic surface-terminated configuration, $GeCH_3$ is expected to show some extraordinary electronic properties. The band structure of $GeCH_3$ was then investigated at the HSE06 level and is shown in Figure 1b. $GeCH_3$ is semiconducting with a direct band gap of 1.76 eV, which is in good accordance with the previous study.[31] This appropriate band gap renders $GeCH_3$ an attractive candidate for electronics. As a comparison, SOC effect was considered during the band structure computation, and the computed band structures are shown in Figure 1b. The band gap of $GeCH_3$ is slightly reduced to be 1.70 eV with weak SOC effect.

To get further insights into the properties of $GeCH_3$, we calculated the partial charge density distribution of the VBM and conduction band minimum (CBM) in $GeCH_3$ monolayer (Figure 2). The VBM (Figure 2a−c) is mainly contributed by

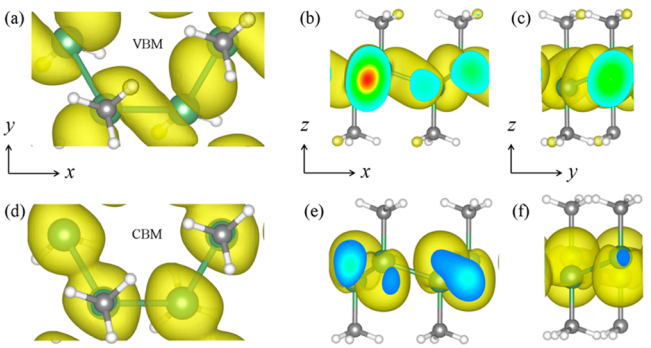


**Figure 2.** Spatial structure of wave functions of VBM (a−c) and CBM (d−f) from the top and side views, respectively, with an isosurface of 0.0025 $e$Å$^{-3}$.

the electronic states of Ge−Ge bonds, while the CBM (Figure 2d−f) is contributed by Ge atoms. Bader charge-transfer analysis demonstrates that there is ∼1.0 lel per atom transferred from Ge to C atoms. Therefore, the surface termination of $CH_3-$ can stabilize germanene with strong Ge−C bonds and can contribute to the high thermal and chemical stability of $GeCH_3$, which have been demonstrated in the previous experimental study.[31]

*Band Structure Engineering via Elastic Strain*. Elastic strain is a well-developed method to engineer the band structures of 2D materials. Therefore, we first investigated the effect of axial tensile strain along $x$ and $y$ directions to tune the band structure of $GeCH_3$. As shown in Figure 3, the band gap of $GeCH_3$ decreases gradually with increasing the tensile strain. The band

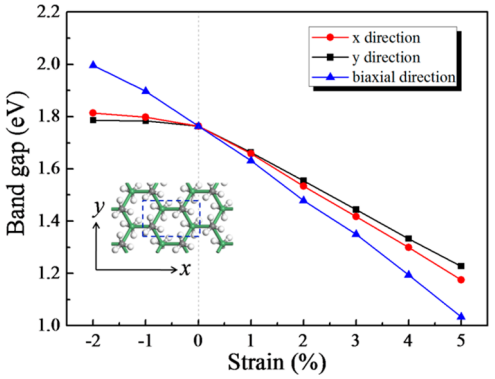


**Figure 3.** Band gap of $GeCH_3$ monolayer as a function of the applied compressive (−2 to 0%) and tensile (0−5%) strain along the $x$ or $y$ axial and biaxial directions.

gap of $GeCH_3$ is more sensitive to the tensile strain in the $x$ direction than to that in the $y$ direction. When a biaxial tensile strain is imposed to the lattice of $GeCH_3$, the band gap of $GeCH_3$ decreases more dramatically. When the applied biaxial strain is as large as 5%, the band gap of $GeCH_3$ is reduced to be 1.03 eV. During the tensile strain modulation, $GeCH_3$ remains to be a direct semiconductor with its band gap decreasing gradually. The phonon spectrum of $GeCH_3$ under 5% biaxial tensile is shown in Figure S1b. There are no imaginary phonon modes in the phonon spectrum indicating the stability of $GeCH_3$ under appropriate tensile strain; however, when a small compressive strain (3%) is applied, the phonon spectrum of $GeCH_3$ (shown in Figure S1d) exhibits appreciable imaginary phonon modes, indicating the instability of $GeCH_3$ under compressive strain. The low stability of $GeCH_3$ under compressive strain can be ascribed to the significant steric effect of $-CH_3$ groups. Therefore, small compressive strain (−2 to 0%) is applied to tune the band gap of $GeCH_3$, and the band gap of $GeCH_3$ increases with increasing the compressive strain along different directions. The band gap of $GeCH_3$ can be enlarged to be ∼2.00 eV under a biaxial compressive strain of −2%. Therefore, applying elastic strain turns out to be effective in tuning the band gap of $GeCH_3$, which could be experimentally achieved flexibly by depositing $GeCH_3$ on an elastic substrate. The strain-tunable band gap of $GeCH_3$ monolayer can be understood in this way. As demonstrated in Figure 2a−f, the VBM and CBM of $GeCH_3$ are contributed by the electron states of Ge−Ge bonds and Ge atoms, respectively. When an elastic strain is applied to the $GeCH_3$ lattice, the Ge−Ge bonds will be elongated, thus resulting in the stretching of electron states and finally contributing to the closing of VBM and CBM.

*Carrier Mobility of $GeCH_3$*. To better estimate the potentials of $GeCH_3$ for electronics, we systematically investigated the electron/hole carrier mobility of $GeCH_3$. Although the SOC effect barely changes the band gap of $GeCH_3$ monolayer, there are two energy levels in the valence band separated or split after the SOC effect is taken into account, as shown in Figure S2a,b. In this case, the effective hole mass of $GeCH_3$ and in consequence the carrier mobility would be changed. Therefore, during the calculation of the effective mass and carrier mobility of $GeCH_3$, the SOC effect was fully considered.



DOI: 10.1021/acs.jpclett.5b01848
J. Phys. Chem. Lett. 2015, 6, 4252−4258

Table 1. Calculated Effective Mass $|m^*|$, DP Constant $E_1$, In-Plane Stiffness $C$, Carrier Mobility $\mu$, and Relaxation Time $\tau$ of $GeCH_3$ along Armchair and Zigzag Directions, with SOC Effect

| direction | | $\lvert m^*\rvert$ ($m_e$) | $\lvert E_1\rvert$ (eV) | $C$ (N/m) | $\mu$ ($cm^2/(V\ s)$) | $\tau$ (fs) |
|---|---|---|---|---|---|---|
| x_armchair | h | $3.67 \times 10^{-2}$ | 6.24 | 51.67 | $1.40 \times 10^4$ | $2.86 \times 10^2$ |
| | e | $2.60 \times 10^{-2}$ | 12.72 | 51.67 | $6.71 \times 10^3$ | 96.98 |
| y_zigzag | h | 0.31 | 6.28 | 49.58 | $1.86 \times 10^2$ | 32.10 |
| | e | 0.19 | 12.47 | 49.58 | $1.25 \times 10^2$ | 13.22 |

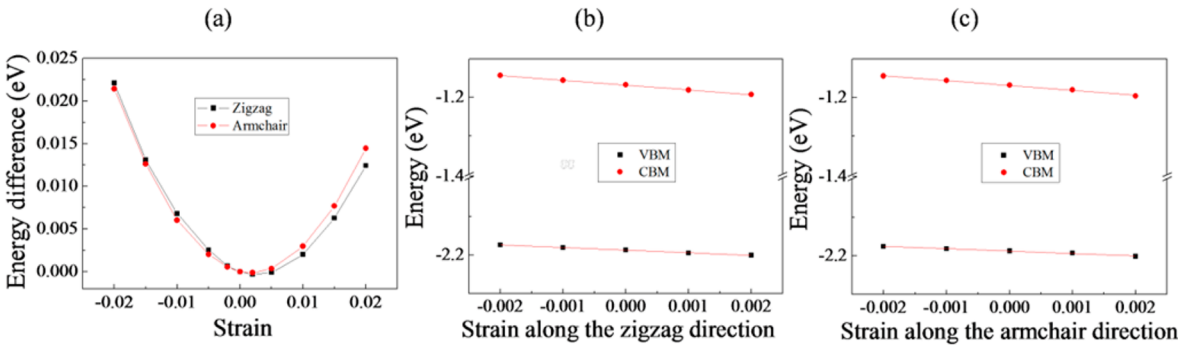


**Figure 4.** Energy difference between the total energy of $GeCH_3$ under uniaxial strain and that of $GeCH_3$ under no strain as a function of the strain along zigzag and armchair directions (a). The in-plane stiffness $C$ can be obtained after fitting the parabola. The energy of VBM and CBM shift with respect to the lattice dilation and compression along zigzag (b) and armchair (c) directions, calculated with SOC effect. The slopes of the straight lines correspond to the DP constant along different directions for electrons and holes.

The effective masses ($m^*$) of the VBM and the CBM along $x$ and $y$ directions were calculated according to $m^* = \hbar^2[\partial^2\epsilon(k)/\partial k^2]^{-1}$. The calculated $|m^*|$ for VBM ($|m^*_h|$) and CBM ($|m^*_e|$) along the $x$ (armchair) direction are $3.67 \times 10^{-2}$ $m_e$ and $2.60 \times 10^{-2}$ $m_e$ ($m_e$ is the electron rest mass), respectively. In the $y$ (zigzag) direction, the calculated $|m^*_h|$ and $|m^*_e|$ are 0.31 $m_e$ and 0.19 $m_e$, respectively, as illustrated in Table 1. The small effective masses in the armchair direction could promise high carrier mobility for $GeCH_3$ in this direction. To better understand the effect of SOC on the properties of $GeCH_3$, we show in Table S1 a comparison of the effective masses with and without SOC effect. It can be found that the SOC effect barely changed the effective electron mass but significantly altered the heavy hole and light hole masses of $GeCH_3$ and made them identical.

After simulating the total energy ($E$) change activated by the applied uniaxial strain ($\delta$), as shown in Figure 4a, we can obtain the in-plane stiffness via $C = [\partial^2 E/\partial\delta^2]/S_0$. Here $S_0$ is the area of the optimized supercell. As a result, the calculated $C$ values along the armchair and zigzag directions are 51.67 and 49.58 N/m, respectively, as exhibited in Table 1. Figure 4b,c shows the energy change of VBM and CBM band edge of $GeCH_3$ with the applied strain along $x$ and $y$ directions, respectively. By simulating the linear relation of band edge energy ($E_{edge}$) and strain ($\delta$) exerted to $x$ and $y$ directions, we can obtain the DP constant $E_1$ ($= dE_{edge}/d\delta$), also presented in Table 1. As a result, the absolute DP constant $E_1$ for electrons (12.72 eV for armchair; 12.47 eV for zigzag) is larger than those for holes (6.24 eV for armchair; 6.28 eV for zigzag). As shown in Figure 2, it can be found that the wave functions of CBM are more delocalized than those of VBM. Thus, small structure deformation due to longitudinal phonon oscillations will more greatly affect the wave functions of CBM than the wave functions of VBM. Therefore, the absolute value of $E_1$ for CBM (electrons) is larger than that for VBM (holes) along the armchair and zigzag directions.

On basis of the calculated $m^*$, $E_1$, and $C$, the carrier mobility for electrons and holes along the armchair and zigzag directions can be obtained through eq 1, and is exhibited in Table 1. Inspiringly, $GeCH_3$ shows high carrier mobility of about $1.40 \times 10^4$ and $6.71 \times 10^3$ $cm^2/(V\ s)$ for holes and electrons along the armchair direction, which are rather superior to those of $MoS_2$ and comparable to those of phosphorene monolayers;[18,19] however, few-layer phosphorene shows low stability and can be easily oxidized at ambient atmosphere.[44] Therefore, the good stability and high carrier mobility make $GeCH_3$ rather desirable for thin-film transistors. Nevertheless, in the zigzag direction, the carrier mobility for holes and electrons are only (1.86 and 1.25) $\times 10^2$ $cm^2/(V\ s)$, respectively. Therefore, $GeCH_3$ shows anisotropic carrier mobility along the armchair and zigzag directions, and the hole and electron mobility along the armchair direction are about a hundred times higher than those along the zigzag directions. The relaxation time ($\tau$) that can reflect how quickly the carriers can restore their equilibrium distribution via scattering with phonons is determined according to $\tau = \mu m^*/e$ and complied in Table 1. As expected, the $\tau$ in the armchair direction is about 10 times higher than that in the zigzag direction. The large carrier mobility and high relaxation time in the armchair direction can be attributed to the small effective mass of this direction, and the high hole mobility also originates from the small deformation potential constant $E_1$ of the VBM.

*Stacking Effects.* Thickness and stacking effect were taken into account in this work to get further insights into the properties of $GeCH_3$. As demonstrated in previous studies, the thickness and stacking order can significantly affect the properties of 2D materials, such as graphene, $MoS_2$, and phosphorene.[19,45,46] For example, the band gap of $MoS_2$ monolayer can decrease with increasing the layer thickness,[47] and different stacking orders can contribute to different band structures of phosphorene.[48] Therefore, $GeCH_3$ bilayer with possible stacking orders was simulated here. As shown in Figure S3, there are four possible stacking configurations for $GeCH_3$ bilayer, including AA


DOI: 10.1021/acs.jpclett.5b01848
J. Phys. Chem. Lett. 2015, 6, 4252−4258

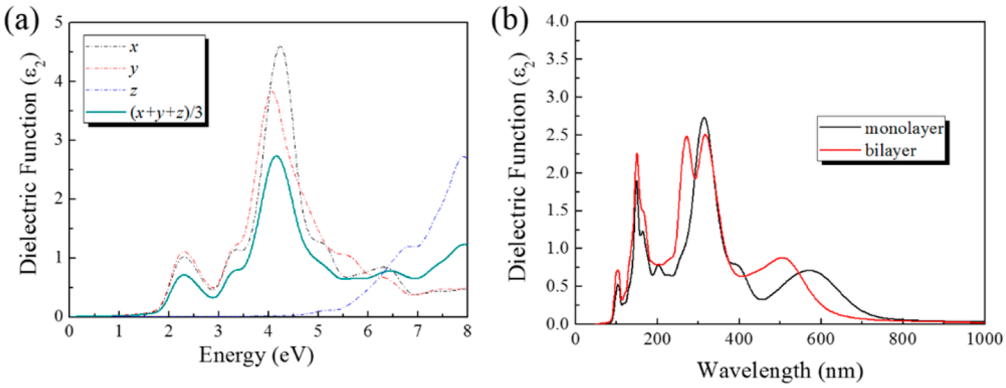


**Figure 5.** (a) Computed imaginary dielectric functions versus energy for $GeCH_3$ monolayer along different incident light directions. (b) Imaginary dielectric functions versus wavelength for $GeCH_3$ monolayer and bilayer in an orthogonal cell at the average level.

stacking, AA′ stacking, AB stacking, and AB′ stacking. The binding energy ($E_{bind}$) of $GeCH_3$ bilayer in different stacking ways is calculated according to $E_{bind} = (E_{bilayer} - 2 \times E_{monolayer})/S_{cell}$, where $E_{bilayer}$ is the total energy of $GeCH_3$ bilayer, $E_{monolayer}$ is the total energy of $GeCH_3$ monolayer, and $S_{cell}$ is the area of the cell. The most stable bilayer configuration is determined by comparing $E_{bind}$, which turns out to be the structure in AB stacking with the binding energy of 0.13 J/m$^2$ and interlayer distance of 0.79 nm, as shown in Figure S3e,f. The binding energy of $GeCH_3$ bilayer in AB stacking with the variation of interlayer distance can be found in Figure S4. Details of the binding energies and interlayer distance of different $GeCH_3$ bilayer configurations are shown in Table S2. Because the binding energy of $GeCH_3$ bilayer is comparable to that of graphene (0.19 J/m$^2$),[49] it would be facile to exfoliate $GeCH_3$ monolayer from its bulk counterpart.

Compared with $GeCH_3$ monolayer, more bands appear in the band structure of bilayer $GeCH_3$ (Figure S5c) due to the band combination from two separate layers; however, the significant band overlapping results in bare changes in the band structure of $GeCH_3$ bilayer. As computed at the HSE06 level, the band gap of $GeCH_3$ bilayer is 1.72 eV, which is only 0.04 eV smaller than that of $GeCH_3$ monolayer (1.76 eV). Therefore, multilayer stacking contributes little effect to the band structure of $GeCH_3$.

*Optical Properties*. Attracted by the appropriate band gap and fantastic electronic properties of $GeCH_3$, we further explored the light absorption of $GeCH_3$ by calculating the imaginary parts of the dielectric function on the basis of eq 2. As shown in Figure 5a, $GeCH_3$ monolayer shows absorption starting at ∼1.5 eV, and there appear two main absorption peaks at ∼2.3 and ∼4.2 eV, corresponding to significant light absorption at the visible and ultraviolet region of solar spectrum, respectively. As illustrated by the solid and dashed lines in Figure 5a, the incident light can be effectively absorbed from the $x$ and $y$ directions. As shown in Figure 5b, both $GeCH_3$ monolayer and bilayer present significant absorption in the range of visible and ultraviolet light. Therefore, 2D $GeCH_3$ nanosheets can be rather attractive for efficient light harvesting and have quite promising applications in optoelectronics.

To summarize, we have investigated the electronic and optical properties of $GeCH_3$ monolayer and bilayer through the computations at the HSE06 level. $GeCH_3$ is an attractive semiconductor with a direct band gap of 1.76 eV, which can be tuned by applying elastic strain. Because of the anisotropic configuration, $GeCH_3$ shows anisotropic electronic properties. With non-negligible SOC effect, $GeCH_3$ exhibits ultrahigh hole mobility (∼1.40 × 10$^4$ cm$^2$/(V s)) in the armchair direction, which is much higher than that of $MoS_2$ and comparable to that of phosphorene. Besides the fantastic electronic properties, $GeCH_3$ monolayer also shows pronounced absorption in the visible and ultraviolet spectrum and exhibits high potential for light harvesting. Because $GeCH_3$ has feeble interlayer interactions, few-layer $GeCH_3$ can sustain identical electronic and optical properties to those of the monolayer. Good stability, appropriate band gap, high hole mobility, and excellent light absorption render $GeCH_3$ nanosheets great applications in electronics and optoelectronics. We hope our computations can help better understand the intrinsic properties and potentials of $GeCH_3$ and promote the development of novel 2D materials.

## ■ ASSOCIATED CONTENT

### Supporting Information

The Supporting Information is available free of charge on the ACS Publications website at DOI: 10.1021/acs.jpclett.5b01848.

Description of $GeCH_3$ including phonon spectrum and band structure of $GeCH_3$ in a hexagonal primitive cell, as well as atomic configurations and band structure of $GeCH_3$ bilayer. (PDF)

## ■ AUTHOR INFORMATION

### Corresponding Author

*E-mail: zhouzhen@nankai.edu.cn.

### Notes

The authors declare no competing financial interest.

## ■ ACKNOWLEDGMENTS

This work was supported by NSFC (21273118) and MOE Innovation Team (IRT13022) in China. The computations were performed on Magic Cube at Shanghai Supercomputer Center.

## ■ REFERENCES

(1) Geim, A. K.; Novoselov, K. S. The Rise of Graphene. *Nat. Mater.* **2007**, *6*, 183−191.

(2) Rao, C. N. R.; Sood, A. K.; Subrahmanyam, K. S.; Govindaraj, A. Graphene: the New Two-Dimensional Nanomaterial. *Angew. Chem., Int. Ed.* **2009**, *48*, 7752−7778.

(3) Allen, M. J.; Tung, V. C.; Kaner, R. B. Honeycomb Carbon: a Review of Graphene. *Chem. Rev.* **2010**, *110*, 132−145.

(4) Georgakilas, V.; Otyepka, M.; Bourlinos, A. B.; Chandra, V.; Kim, N.; Kemp, K. C.; Hobza, P.; Zboril, R.; Kim, K. S. Functionalization of



DOI: 10.1021/acs.jpclett.5b01848
*J. Phys. Chem. Lett.* 2015, 6, 4252−4258

Graphene: Covalent and Non-Covalent Approaches, Derivatives and Applications. *Chem. Rev.* **2012**, *112*, 6156−6214.
(5) Tang, Q.; Zhou, Z. Graphene-Analogous Low-Dimensional Materials. *Prog. Mater. Sci.* **2013**, *58*, 1244−1315.
(6) Jing, Y.; Zhou, Z.; Cabrera, C. R.; Chen, Z. Graphene, Inorganic Graphene Analogs and Their Composites for Lithium Ion Batteries. *J. Mater. Chem. A* **2014**, *2*, 12104−12122.
(7) Novoselov, K. S.; Geim, A. K.; Morozov, S. V.; Jiang, D.; Zhang, Y.; Dubonos, S. V.; Grigorieva, I. V.; Firsov, A. A. Electric Field Effect in Atomically Thin Carbon Films. *Science* **2004**, *306*, 666−669.
(8) Novoselov, K. S.; Geim, A. K.; Morozov, S. V.; Jiang, D.; Katsnelson, M. I.; Grigorieva, I. V.; Dubonos, S. V.; Firsov, A. A. Two-Dimensional Gas of Massless Dirac Fermions in Graphene. *Nature* **2005**, *438*, 197−200.
(9) Tang, Q.; Zhou, Z.; Chen, Z. F. Graphene Related Materials: Tuning Properties by Functionalization. *Nanoscale* **2013**, *5*, 4541−4583.
(10) Sofo, J. O.; Chaudhari, A. S.; Barber, G. D. Graphane: a Two-Dimensional Hydrocarbon. *Phys. Rev. B: Condens. Matter Mater. Phys.* **2007**, *75*, 153401.
(11) Cheng, S.-H.; Zou, K.; Okino, F.; Gutierrez, H. R.; Gupta, A.; Shen, N.; Eklund, P.; Sofo, J.; Zhu, J. Reversible Fluorination of Graphene: Evidence of a Two-Dimensional Wide Bandgap Semiconductor. *Phys. Rev. B: Condens. Matter Mater. Phys.* **2010**, *81*, 205435.
(12) Li, Y.; Li, F.; Chen, Z. Graphane/Fluorographene Bilayer: Considerable C−H···F−C Hydrogen Bonding and Effective Band Structure Engineering. *J. Am. Chem. Soc.* **2012**, *134*, 11269−11275.
(13) Tang, Q.; Zhou, Z.; Chen, Z. Innovation and Discovery of Graphene-Like Materials via DFT Computations. *WIREs Comput. Mol. Sci.* **2015**, *5*, 360−379.
(14) Jing, Y.; Tan, X.; Zhou, Z.; Shen, P. Tuning Electronic and Optical Properties of $MoS_2$ Monolayer via Molecular Charge Transfer. *J. Mater. Chem. A* **2014**, *2*, 16892−16897.
(15) Tang, Q.; Zhou, Z.; Shen, P. Are MXenes Promising Anode Materials for Li Ion Batteries? Computational Studies on Electronic Properties and Li Storage Capability of $Ti_3C_2$ and $Ti_3C_2X_2$ (X = F, OH) Monolayer. *J. Am. Chem. Soc.* **2012**, *134*, 16909−16916.
(16) Jing, Y.; Tang, Q.; He, P.; Zhou, Z.; Shen, P. Small Molecules Make Big Differences: Molecular Doping Effects on Electronic and Optical Properties of Phosphorene. *Nanotechnology* **2015**, *26*, 095201.
(17) Ziletti, A.; Huang, S. M.; Coker, D. F.; Lin, H. Van Hove Singularity and Ferromagnetic Instability in Phosphorene. *Phys. Rev. B: Condens. Matter Mater. Phys.* **2015**, *92*, 085423.
(18) Cai, Y.; Zhang, G.; Zhang, Y. W. Polarity-Reversed Robust Carrier Mobility in Monolayer $MoS_2$ Nanoribbons. *J. Am. Chem. Soc.* **2014**, *136*, 6269−6275.
(19) Qiao, J.; Kong, X.; Hu, Z. X.; Yang, F.; Ji, W. High-Mobility Transport Anisotropy and Linear Dichroism in Few-Layer Black-Phosphorus. *Nat. Commun.* **2014**, *5*, 4475.
(20) Shao, Z.-G.; Ye, X.-S.; Yang, L.; Wang, C.-L. First-Principles Calculation of Intrinsic Carrier Mobility of Silicene. *J. Appl. Phys.* **2013**, *114*, 093712.
(21) Houssa, M.; Pourtois, G.; Afanas'ev, V.; Stesmans, A. Electronic Properties of Two-Dimensional Hexagonal Germanium. *Appl. Phys. Lett.* **2010**, *96*, 082111.
(22) Liu, C.-C.; Feng, W.; Yao, Y. Quantum Spin Hall Effect in Silicene and Two-Dimensional Germanium. *Phys. Rev. Lett.* **2011**, *107*, 076802.
(23) Matthes, L.; Pulci, O.; Bechstedt, F. Massive Dirac Quasiparticles in the Optical Absorbance of Graphene, Silicene, Germanene, and Tinene. *J. Phys.: Condens. Matter* **2013**, *25*, 395305.
(24) Ye, X.-S.; Shao, Z.-G.; Zhao, H.; Yang, L.; Wang, C.-L. Intrinsic Carrier Mobility of Germanene is Larger than Graphene's: First-Principle Calculations. *RSC Adv.* **2014**, *4*, 21216−21220.
(25) Ni, Z.; Liu, Q.; Tang, K.; Zheng, J.; Zhou, J.; Qin, R.; Gao, Z.; Yu, D.; Lu, J. Tunable Bandgap in Silicene and Germanene. *Nano Lett.* **2012**, *12*, 113−118.
(26) Seixas, L.; Padilha, J. E.; Fazzio, A. Quantum Spin Hall Effect on Germanene Nanorod Embedded in Completely Hydrogenated Germanene. *Phys. Rev. B: Condens. Matter Mater. Phys.* **2014**, *89*, 195403.
(27) Bianco, E.; Butler, S.; Jiang, S.; Restrepo, O. D.; Windl, W.; Goldberger, J. E. Stability and Exfoliation of Germanane: a Germanium Graphane Analogue. *ACS Nano* **2013**, *7*, 4414−4421.
(28) Koski, K. J.; Cui, Y. The New Skinny in Two-Dimensional Nanomaterials. *ACS Nano* **2013**, *7*, 3739−3743.
(29) Ghosh, R. K.; Brahma, M.; Mahapatra, S. Germanane: a Low Effective Mass and High Bandgap 2-D Channel Material for Future FETs. *IEEE Trans. Electron Devices* **2014**, *61*, 2309−2315.
(30) Low, K. L.; Huang, W.; Yeo, Y.; Liang, G. Ballistic Transport Performance of Silicane and Germanane Transistors. *IEEE Trans. Electron Devices* **2014**, *61*, 1590−1598.
(31) Jiang, S.; Butler, S.; Bianco, E.; Restrepo, O. D.; Windl, W.; Goldberger, J. E. Improving the Stability and Optical Properties of Germanane via One-Step Covalent Methyl-Termination. *Nat. Commun.* **2014**, *5*, 3389.
(32) Kresse, G.; Hafner, J. Ab initio Molecular Dynamics for Liquid Metals. *Phys. Rev. B: Condens. Matter Mater. Phys.* **1993**, *47*, 558−561.
(33) Blöchl, P. E. Projector Augmented-Wave Method. *Phys. Rev. B: Condens. Matter Mater. Phys.* **1994**, *50*, 17953−17979.
(34) Kresse, G.; Joubert, D. From Ultrasoft Pseudopotentials to the Projector Augmented-Wave Method. *Phys. Rev. B: Condens. Matter Mater. Phys.* **1999**, *59*, 1758−1775.
(35) Perdew, J. P.; Burke, L.; Ernzerhof, M. Generalized Gradient Approximation Made Simple. *Phys. Rev. Lett.* **1996**, *77*, 3865−3868.
(36) Grimme, S. Semiempirical GGA-Type Density Functional Constructed with a Long-Range Dispersion Correction. *J. Comput. Chem.* **2006**, *27*, 1787−1799.
(37) Heyd, J.; Peralta, J. E.; Scuseria, G. E.; Martin, R. L. Energy Band Gaps and Lattice Parameters Evaluated with the Heyd-Scuseria-Ernzerhof Screened Hybrid Functional. *J. Chem. Phys.* **2005**, *123*, 174101.
(38) Segall, M. D.; Lindan, P. J. D.; Probert, M. J.; Pickard, C. J.; Hasnip, P. J.; Clark, S. J.; Payne, M. C. First-Principles Simulation: Ideas, Illustrations and the CASTEP Code. *J. Phys.: Condens. Matter* **2002**, *14*, 2717−2744.
(39) Bardeen, J.; Shockley, W. Deformation Potentials and Mobilities in Non-Polarcrystals. *Phys. Rev.* **1950**, *80*, 72−80.
(40) Zhang, X.; Zhao, X.; Wu, D.; Jing, Y.; Zhou, Z. High and Anisotropic Carrier Mobility in Experimentally Possible $Ti_2CO_2$ (MXene) Monolayer and Nanoribbons. *Nanoscale* **2015**, *7*, 16020−16025.
(41) Long, M.; Tang, L.; Wang, D.; Li, Y.; Shuai, Z. Electronic Structure and Carrier Mobility in Graphdiyne Sheet and Nanoribbons: Theoretical Predictions. *ACS Nano* **2011**, *5*, 2593−2600.
(42) Xie, J.; Zhang, Z. Y.; Yang, D. Z.; Xue, D. S.; Si, M. S. Theoretical Prediction of Carrier Mobility in Few-Layer $BC_2N$. *J. Phys. Chem. Lett.* **2014**, *5*, 4073−4077.
(43) Gajdoš, M.; Hummer, K.; Kresse, G.; Furthmüller, J.; Bechstedt, F. Linear Optical Properties in the Projector-Augmented Wave Methodology. *Phys. Rev. B: Condens. Matter Mater. Phys.* **2006**, *73*, 045112.
(44) Koenig, S. P.; Doganov, R. A.; Schmidt, H.; Castro Neto, A. H.; Özyilmaz, B. Electric Field Effect in Ultrathin Black Phosphorus. *Appl. Phys. Lett.* **2014**, *104*, 103106.
(45) Ohta, T.; Bostwick, A.; McChesney, J. L.; Seyller, T.; Horn, K.; Rotenberg, E. Interlayer Interaction and Electronic Screening in Multilayer Graphene Investigated with Angle-Resolved Photoemission Spectroscopy. *Phys. Rev. Lett.* **2007**, *98*, 206802.
(46) Liu, Q.; Li, L.; Li, Y.; Gao, Z.; Chen, Z.; Lu, J. Tuning Electronic Structure of Bilayer $MoS_2$ by Vertical Electric Field: a First-Principles Investigation. *J. Phys. Chem. C* **2012**, *116*, 21556−21562.
(47) Ellis, J. K.; Lucero, M. J.; Scuseria, G. E. The Indirect to Direct Band Gap Transition in Multilayered $MoS_2$ as Predicted by Screened Hybrid Density Functional Theory. *Appl. Phys. Lett.* **2011**, *99*, 261908.


DOI: 10.1021/acs.jpclett.5b01848
*J. Phys. Chem. Lett.* 2015, 6, 4252−4258

(48) Dai, J.; Zeng, X. C. Bilayer Phosphorene: Effect of Stacking Order on Bandgap and Its Potential Applications in Thin-Film Solar Cells. *J. Phys. Chem. Lett.* **2014**, *5*, 1289−1293.
(49) Liu, Z.; Liu, J. Z.; Cheng, Y.; Li, Z.; Wang, L.; Zheng, Q. Interlayer Binding Energy of Graphite: a Mesoscopic Determination from Deformation. *Phys. Rev. B: Condens. Matter Mater. Phys.* **2012**, *85*, 205418.



DOI: 10.1021/acs.jpclett.5b01848
*J. Phys. Chem. Lett.* 2015, 6, 4252−4258